

# Laboratory-scale experiment to study nonlinear $N$ -wave distortion by thermal turbulence

Édouard Salze<sup>a)</sup>

*Laboratoire de Mécanique des Fluides et d'Acoustique, UMR CNRS 5509, École Centrale de Lyon, Université de Lyon, 36, avenue Guy de Collongue, 69134 Écully Cedex, France*

Petr Yuldashev<sup>b)</sup>

*Department of General Physics and Magneto-Ordered Matter, Faculty of Physics, M.V. Lomonosov Moscow State University, Moscow 119991, Russia*

Sébastien Ollivier

*Laboratoire de Mécanique des Fluides et d'Acoustique, UMR CNRS 5509, Université Lyon 1, Université de Lyon, 43 boulevard du 11 novembre 1918, 69622 Villeurbanne Cedex, France*

Vera Khokhlova

*Department of Acoustics, Faculty of Physics, M.V. Lomonosov Moscow State University, Moscow 119991, Russia*

Philippe Blanc-Benon

*Laboratoire de Mécanique des Fluides et d'Acoustique, UMR CNRS 5509, École Centrale de Lyon, Université de Lyon, 36, avenue Guy de Collongue, 69134 Écully Cedex, France*

(Received 2 August 2013; revised 24 May 2014; accepted 23 June 2014)

The nonlinear propagation of spark-generated  $N$ -waves through thermal turbulence is experimentally studied at the laboratory scale under well-controlled conditions. A grid of electrical resistors was used to generate the turbulent field, well described by a modified von Kármán model. A spark source was used to generate high-amplitude ( $\sim 1500$  Pa) and short duration ( $\sim 50$   $\mu$ s)  $N$ -waves. Thousands of waveforms were acquired at distances from 250 to 1750 mm from the source ( $\sim 15$  to 100 wavelengths). The mean values and the probability densities of the peak pressure, the deviation angle, and the rise time of the pressure wave were obtained as functions of propagation distance through turbulence. The peak pressure distributions were described using a generalized gamma distribution, whose coefficients depend on the propagation distance. A line array of microphones was used to analyze the effect of turbulence on the propagation direction. The angle of deviation induced by turbulence was found to be smaller than  $15^\circ$ , which validates the use of the parabolic equation method to model this kind of experiment. The transverse size of the focus regions was estimated to be on the order of the acoustic wavelength for propagation distances longer than 50 wavelengths. © 2014 Acoustical Society of America. [<http://dx.doi.org/10.1121/1.4887458>]

PACS number(s): 43.28.Gq, 43.25.Cb, 43.28.Mw, 43.25.Jh [ROC]

Pages: 556–566

## I. INTRODUCTION

Acoustic propagation of high-amplitude impulse sound is relevant to different problems: blast waves generated from explosions or gunshots, ultrasonic pulses in focused beams, or the propagation of sonic boom in the atmosphere. This last example is well documented in the literature since the late 1950s. Randomly distorted sonic booms waveforms with variable pressure levels and rise times outdoor measurements have been recorded.<sup>1</sup> The atmospheric turbulence is responsible for the random variability of sonic boom waveforms.<sup>2–4</sup> Time domain filters have been used to describe this variability.<sup>5</sup> To evaluate the influence of the

turbulent layer, a statistical analysis of the acoustic  $N$ -wave distortion through the turbulent layer is needed. However, field measurements suffer from a lack of control on atmosphere characteristics. The small number of aircraft flight tests for fixed atmospheric conditions limits the statistical analysis of the effects of turbulence. Numerical simulations would be an alternative, but the computational cost of long range nonlinear propagation of shockwaves through realistic turbulence still limits this approach to two-dimensional models, or require strong approximations, therefore experiments are still necessary.

To experimentally investigate the propagation of  $N$ -waves through turbulence, an alternative to outdoor measurements is to perform downscaled experiments under well-controlled laboratory conditions. Laboratory experiments allow the study of the propagation with or without turbulence, which helps to identify the effects purely related to the propagation through the turbulent layer. To study the effect of a local sound speed inhomogeneity on shockwaves,

<sup>a)</sup>Author to whom correspondence should be addressed. Electronic mail: [edouard.salze@ec-lyon.fr](mailto:edouard.salze@ec-lyon.fr)

<sup>b)</sup>Also at: Laboratoire de Mécanique des Fluides et d'Acoustique, UMR CNRS 5509, École Centrale de Lyon, Université de Lyon, 36, avenue Guy de Collongue, 69134 Écully Cedex, France.

experiments have been performed in water with scatterers.<sup>6</sup> Performing experiments in water allows the downscaling of linear dissipation. However, fully developed turbulence cannot be easily generated in a water-tank, and high amplitude impulse waves in water lead to cavitation phenomena.

The present study was performed in air. The turbulent field was generated by a grid of resistors, and short duration high amplitude pressure *N*-waves were produced using a spark source. In laboratory-scale experiments in air, typical propagation distances are on the order of 1 m, turbulence larger scales are on the order of 10–20 cm. The acoustic wavelength is on the order of one to 2 cm, which corresponds to a wave duration on the order of tens of microseconds.<sup>7–9</sup> Comparing experiments in air at laboratory scale to sonic boom propagation in the atmosphere, a geometrical scaling factor of about 1/1000 is obtained for propagation distances, turbulence length scales, and wave duration. Since the durations of spark-generated *N*-waves are much shorter than blast waves or sonic booms durations, the spectrum of an *N*-wave is in a higher frequency domain. This leads to a large increase of linear absorption, and also to different contributions of the relaxation effects. Therefore, to observe significant nonlinear effects, and to obtain a sharp shock structure with a front shock rise time much shorter than wave duration, the pressure level must be much higher than sonic boom peak pressure. Nevertheless, laboratory-scale experiments including propagation through a turbulent layer permit us to observe waveform distortions similar to those observed with real sonic booms, namely unaltered *N*-waves, high-amplitude *U*-waves, waveforms with very large rise times, and rounded or messy waves.<sup>9,10</sup>

The propagation of short duration *N*-waves through kinematic turbulence generated by jets has been experimentally studied by Lipkens,<sup>8,10</sup> Ollivier,<sup>11</sup> and then by Averyanov.<sup>9</sup> Those studies showed that initial *N*-waves are distorted and that, on average, the peak pressure is decreased and the rise time of the front shock is increased after propagation through turbulence. These effects are more significant when increasing the turbulent intensity level (by increasing the jet velocity). However, if the propagation distance through turbulence is longer than the distance of occurrence of first caustics, the wave can also be focused by random inhomogeneities, leading to some *U*-shaped waves with short rise times and peak pressures amplified more than three times the pressure recorded without turbulence for the same propagation distance. To study the influence of the turbulence level, Averyanov varied the velocity of a jet. He showed that the peak pressure probability densities can be fitted by generalized gamma laws, whose parameters depend on the turbulence level for a fixed propagation distance.<sup>9</sup> The study of the influence of the propagation distance using jets is more difficult due to experimental constraints. If the source and the microphones are on both sides of the jet and the width is varied, the ratio between the shear layer width and the fully developed turbulent field width is not constant.<sup>8</sup> If the source or the microphone is moved into the jet to vary the propagation distance, their behavior is influenced by the flow.<sup>9</sup> To investigate the influence of the distance, it is therefore more convenient to use thermal turbulence generated by

a heated grid of resistors. Although scalar-type thermal turbulence differs from vector-type kinematic turbulence, similar distortions and focusing effects are observed. Long distance sound propagation through thermal turbulence has been previously studied by some of the present authors<sup>11</sup> but the analysis of data was limited by uncertainties on the source and on the microphone response to shockwaves.

Taking advantage of a better knowledge of the pressure *N*-waves generated by the spark source,<sup>12,13</sup> together with new experimental facilities, a new experiment has been performed in order to study the influence of the propagation distance through thermal turbulence.<sup>14,15</sup> In the present paper, statistics of *N*-waves parameters are presented for increasing propagation distance. Using a line array of seven microphones, evidence of focusing effect is shown, the transverse size of the focusing area is estimated, and the random fluctuation of the angle of arrival is analyzed. Although it was not possible to measure accurately the front shock rise time using 1/8-in. microphones, the statistics of the front shock rise time are given to show the influence of the propagation distance through turbulence on the increase of this parameter. In order to emphasize that the microphones frequency response must be considered when analyzing the rise time statistics, data simultaneously measured with a 1/8- and a 1/4-in. microphone are compared. This paper is organized as follows. The experimental setup is detailed in Sec. II, then results are given and discussed in Sec. III.

## II. EXPERIMENTAL METHOD

### A. Experimental setup

A schematic of the experiment is drawn in Fig. 1. Random sound speed inhomogeneities were generated by using a 4.4 m × 1.1 m heating grid of electrical resistors dissipating a total electrical power of 64 kW. Resistors were arranged to form a 9 cm square mesh grid. Fully developed thermal turbulent field was obtained 160 cm above the grid by mixing of thermal plumes. An electrical spark source was used to generate short duration and high pressure spherical *N*-waves.<sup>15</sup> The spark source was made of two tungsten electrodes, separated by a gap of 20 mm, connected to an electrical supply. A high voltage electrical source (16–20 kV) was used to charge condensers until the potential breakdown of

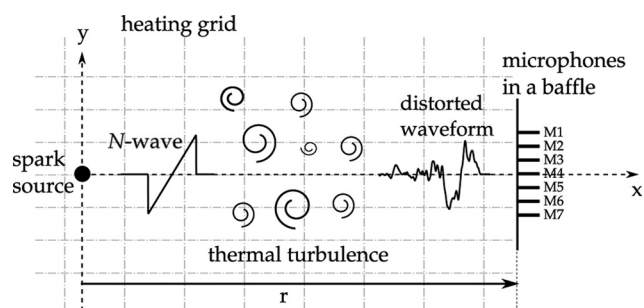


FIG. 1. Schematic of the experiment (top view). The initial *N*-wave is altered during its propagation through thermal turbulence and is measured at a distance *r* from the spark source using a line array of seven microphones flush-mounted into a baffle.

air was reached, then a spark was generated. The sudden local heating generates a high amplitude and short duration pressure pulse. The voltage value was set to obtain a spark approximately every 1 s. Because of nonlinear propagation, an  $N$ -wave was formed a few centimeters away from the electrodes.

Acoustic waves were recorded after propagation through thermal turbulence using a line array of seven equally spaced 1/8-in. condenser microphones (three Brüel & Kjær type 4138 and four G.R.A.S. type 40DP). Microphones were flush-mounted without their protection grid into a plane baffle in order to limit diffraction on the edges of the microphones. The baffle dimensions were 30 cm  $\times$  20 cm, which allowed us to delay the measurement of waves diffracted on the edge of the baffle by more than six times the duration of the wave. The distance between neighbor microphones was set either to 1 or 2 cm. The line array of microphones was mounted perpendicularly to the propagation path. The central microphone therefore measured the incoming waves at normal incidence. The source-microphones distance  $r$  was remote-controlled using a motorized device. Two Brüel & Kjær Nexus amplifiers with an extended frequency response were used ( $-3$  dB cutoff at 200 kHz). The seven microphone signals were simultaneously recorded at a sampling frequency of 10 MHz using a 12 bit National Instruments digital acquisition card. Experiments were performed in an anechoic chamber. The temperature was monitored during the acoustical measurements using a thermocouple placed near the microphones baffle.

## B. Characteristics of spark-generated pressure $N$ -waves

The characteristics of spark-generated  $N$ -waves have been previously studied in details in the literature<sup>16–20</sup> and by the present authors.<sup>12,13,21</sup> Hereafter, the main features of the source used in the present study are given. The main parameters of the wave discussed hereafter are the maximum positive peak pressure of the wave  $P_{\max}$ , and the rise time  $\tau$  of the front shock (see Fig. 2).

The rise time is defined here as the time interval during which the pressure rises from 10% to 90% of the positive peak pressure  $P_{\max}$ . As shown in Fig. 2, at a distance  $r = 20$

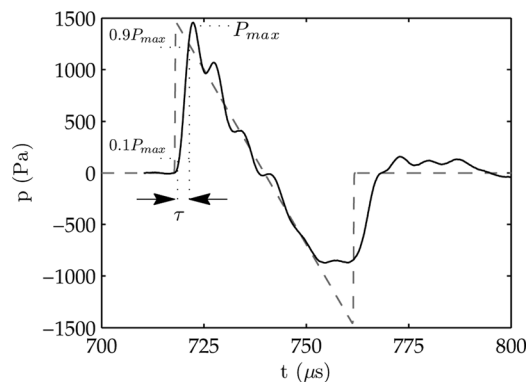


FIG. 2. —: pressure waveform measured at  $r = 200$  mm from the source, ---: corresponding ideal  $N$ -wave. The parameter  $P_{\max}$  is defined as the maximum positive peak pressure. The parameter  $\tau$  is defined as the rise time from 10% to 90% of  $P_{\max}$ .

cm from the spark source, the waveform is close to an  $N$ -wave. At this distance, the peak pressure is about 1500 Pa ( $\pm 12$  Pa), the half-duration is about 20  $\mu$ s ( $\pm 0.5$   $\mu$ s), the rise time estimation is on the order of 3  $\mu$ s ( $\pm 10$  ns), and the wavelength is about 17 mm. Similarly to blast waves, the wave is not symmetrical, and the negative peak pressure amplitude is lower than the positive peak pressure. Other differences between the measured waveform and the corresponding ideal  $N$ -wave shown in Fig. 2 are mainly due to the microphone frequency response. The frequency response of the microphones used in the present study is limited to 140 kHz, which caused an overestimation of the rise time  $\tau_{\text{ref}}$ . Actually, it is known from optical measurements that the pressure rise time is on the order of 0.4  $\mu$ s at  $r = 1$  m for this pressure amplitude,<sup>13</sup> whereas the minimum value obtained using 1/8-in. microphones is 2.6  $\mu$ s. Rise time estimations on the order of 3  $\mu$ s therefore correspond to the rise time of the microphones rather than to the pressure rise time. Despite these limitations of available microphones, the rise time is discussed hereafter since significant increases of the rise time were observed with turbulence. The oscillations seen on the output voltage of the microphone correspond to its resonance.<sup>18,22</sup> Depending on the microphone, the period of these oscillations was found to be on the order of 6–7  $\mu$ s.

Peak pressure and rise time mean values, together with their corresponding standard deviations ( $\sigma$ ), computed over 100 spark shots, are given as a function of source-microphone distance  $r$  (Table I). As previously reported, these values are consistent with numerical simulations of the nonlinear propagation of spherical  $N$ -waves.<sup>13</sup> Peak pressure and rise time mean values measured without turbulence, respectively named  $P_{\text{ref}}$  and  $\tau_{\text{ref}}$ , are used in the next sections as reference values to compare the data obtained with turbulence. Without turbulence, the decrease of the peak pressure with the distance is due to a combination of spherical spreading of the pressure wave, linear absorption, relaxation, and nonlinear effects.<sup>12,19</sup>

## C. Thermal turbulence

The field of thermal turbulence was characterized using constant current temperature probes and thermocouples. A mean temperature  $T_{\text{mean}}$  of 308 K, and root mean square

TABLE I. Mean values and standard deviations of the maximum positive peak pressure and of the rise time as functions of distance, without turbulence.

$r$ (mm)	$P_{\text{ref}}$ (Pa)	$\sigma_{P_{\text{ref}}}$ (%)	$\tau_{\text{ref}}$ ( $\mu$ s)	$\sigma_{\tau_{\text{ref}}}$ (ns)
250	1170	1.33	2.59	16
400	675	1.91	2.62	14
550	460	1.67	2.64	16
700	350	2.11	2.66	17
850	280	2.18	2.68	24
1000	225	2.02	2.70	12
1150	190	2.02	2.72	21
1300	165	1.38	2.74	18
1450	140	1.62	2.78	19
1600	130	1.31	2.81	22
1750	115	1.85	2.82	25

temperature fluctuations  $T_{\text{rms}}$  of 5 K was measured, leading to about 0.8% root mean square fluctuations of the refraction index  $\mu_{\text{rms}} = T_{\text{rms}}/2T_{\text{mean}}$ , which is 0.8% of sound celerity standard deviation. By means of correlations measurements in the horizontal and vertical directions, the turbulence outer scale  $L_0$  was found to be 15 cm, and the vertical convection speed  $U_z$  of the turbulent structures was 1.1 m/s. To characterize thermal turbulence, the temperature fluctuation as a function of time was first measured, then the frequency spectrum  $G_{\text{meas}}(f)$  was computed. Assuming the Taylor hypothesis,<sup>23</sup> the corresponding one-dimensional spectrum  $G_{\text{1D,exp}}(K)$  as a function of the turbulent wavenumber  $K$  is obtained from the measured spectrum  $G_{\text{meas}}(f)$  using the following relations:  $K = 2\pi f/U_z$  and  $G_{\text{1D,exp}}(K) = U_z/2\pi G_{\text{meas}}(f)$ . The spectrum of temperature fluctuations in the experiment was compared to a modified von Kármán model of energy spectrum  $G_{\text{vK}}(K)$  defined as a function of the turbulent wavenumber  $K$  by Eq. (1),

$$G_{\text{vK}}(K) = C\mu_{\text{rms}}^2 \frac{K^2 \exp(-K^2/K_m^2)}{L_0^{2/3} (K^2 + K_0^2)^{11/6}}, \quad (1)$$

where  $\mu_{\text{rms}}$  is the root mean square fluctuations of the refraction index,  $K_0 = 1/L_0$ ,  $L_0$  is the outer scale of turbulence and  $K_m = 5.92/l_0$ ,  $l_0$  is the inner scale of turbulence related to the high wavenumber cutoff of the spectrum, and  $C = 0.7924$  is a constant. The corresponding one-dimensional model spectrum  $G_{\text{1D,vK}}$  is obtained by integrating the energy spectrum<sup>23</sup>

$$G_{\text{1D,vK}}(K) = \frac{1}{2} \int_K^\infty \frac{G_{\text{vK}}(K')}{K'} dK'. \quad (2)$$

The model spectrum  $G_{\text{1D,vK}}$  was computed using the measured values of  $\mu_{\text{rms}}$  and  $L_0$ , and compared to the experimental one-dimensional spectrum  $G_{\text{1D,exp}}$  (Fig. 3). The inner scale  $l_0$  was not measured but estimated on the order of 6 mm by fitting the spectrum in the high wavenumber range.

As previously reported in the literature for the same experimental facility,<sup>11,35</sup> an excellent agreement was found between the experimental one-dimensional spectrum  $G_{\text{1D,exp}}$  and the corresponding model spectrum  $G_{\text{1D,vK}}$ . In the

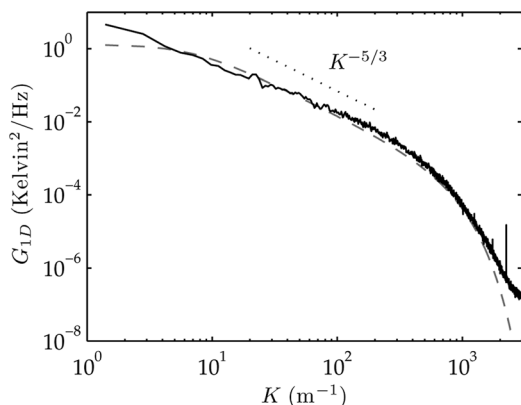


FIG. 3. One-dimensional spectrum of temperature fluctuations. —: measured spectrum  $G_{\text{1D,exp}}$ , ---: von Kármán model spectrum  $G_{\text{1D,vK}}$ .

perspective of the comparison with numerical simulations of wave propagation through random media, the ability to experimentally obtain this kind of turbulence spectrum is interesting because it can be easily synthesized.<sup>24,25</sup>

### III. RESULTS AND DISCUSSION

#### A. Waveform distortion

In this section, interest is focused on waveform distortion. In Fig. 4 are given examples of waveforms measured by one microphone after propagation through turbulence, together with the wave measured at the same distance without turbulence. These waveforms were measured at the distance  $r = 1600$  mm from the spark source for different spark shots, therefore each waveform stands for different states of the propagation medium. The pressure level in the waveforms was normalized by  $P_{\text{ref}}$  previously defined as the positive peak pressure level measured at the same distance without turbulence (Table I). It was checked that the 200  $\mu\text{s}$  systematic shift between the arrival times observed with and without turbulence is due to the increase of the mean temperature by the heating grid of resistors. Additional random fluctuation of arrival times is due to the deviation of propagation paths by sound speed inhomogeneities. Similarly to typical sonic boom profiles measured in the atmosphere,<sup>1,3,26</sup> strongly distorted waveforms are observed:  $U$ -wave pulses with high amplitude and narrow shock fronts [Fig. 4(a)], waves with several shocks [Fig. 4(b)], waves with long rise times [Fig. 4(c)], rounded waves with low amplitude [Fig. 4(d)]. Waves with a positive peak pressure on their tail part were also observed. Note that at this distance ( $r = 1600$  mm), the unaltered  $N$ -wave was also observed, however this case is not shown here.

The corresponding spectra amplitudes were plotted in Fig. 5, where the 0 dB level is the maximum of the spectrum obtained without turbulence. In the case of  $U$ -waves with very high amplitudes, an amplification of approximately 7 dB was found above 40 kHz [Fig. 5(a)]. The cutoff of the

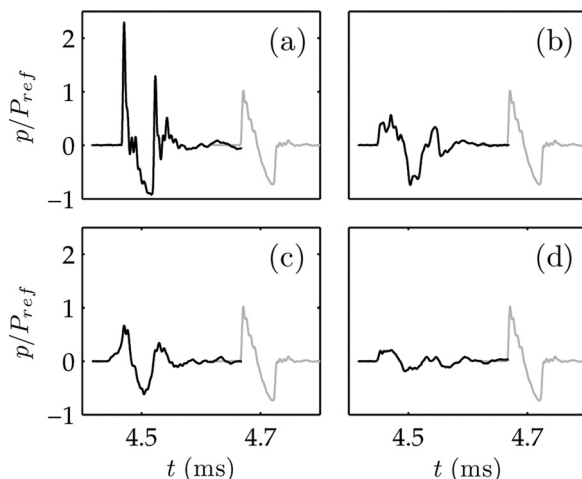


FIG. 4. Four examples of waveforms measured at the same distance  $r = 1600$  mm from the source. —: reference waveform measured without turbulence, - - -: examples of waveforms measured with turbulence. Amplitudes are normalized by the reference pressure level  $P_{\text{ref}}(r)$  measured without turbulence (see Table I).

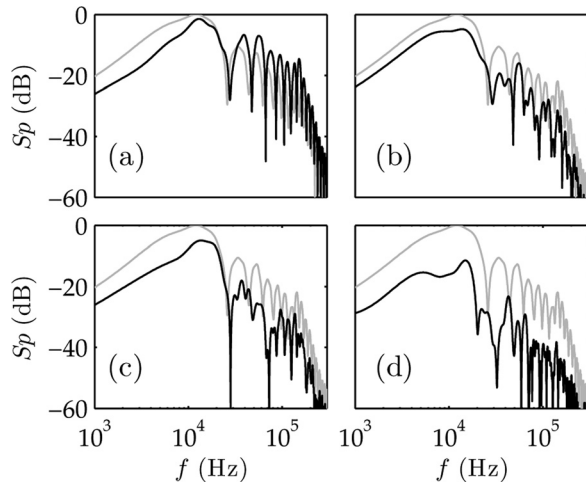


FIG. 5. Spectra of the waveforms given in Fig. 4. —: spectrum of the reference waveform, without turbulence. —: spectra of the waveforms measured with turbulence, at the same distance  $r = 1600$  mm from the source. Spectra amplitudes are normalized by the maximum of the reference spectrum measured without turbulence.

microphone and amplifier response above 140 kHz is clearly seen, and the level was probably amplified at high frequencies well over the microphone bandwidth. The three other waves [Figs. 5(b)–5(d)] mainly differ from the  $N$ -wave by attenuation in the whole frequency range, and local minima caused by interferences between delayed arrivals.

High level  $U$ -waves are focused  $N$ -waves. It is known from numerical simulations<sup>25,27,28</sup> that, outside the focus region, waveforms present multiple arrivals because of wavefront folding. Using a shock tube and a schlieren optical method, Hesselink<sup>29</sup> has observed wavefront folding of weak shocks that propagate through an inhomogeneous mixing of helium and dichlorodifluoromethane. However, in turbulent air, it would be difficult to visualize shock waves using schlieren technique because heating induces higher air density gradients than acoustic waves do. In the present experiment, pressure waveforms were measured in the vicinity of a focus region using the line array of seven microphones separated by a distance of 1 or 2 cm in the  $y$ -direction. Figure 6 shows an example of waveform recorded simultaneously with the seven microphones separated by 1 cm. Waveforms were plotted as functions of the distance instead of time using the mean sound speed deduced from the temperature measurement. The normalized pressure level  $p(x, y)/P_{\text{ref}}$  is in the range  $[-2; 3]$ . The microphone number 6, located at  $y = -40$  mm, recorded an  $U$ -wave with a peak positive pressure amplified by a factor of 2.5, with respect to values in quiescent air, which is a typical amplification factor observed for  $U$ -shaped waveforms. The peak pressure decreases from microphone 5 to 1, the peak pressure level microphone 1 is about 0.8 times the reference level.

The waveforms obtained from the microphones have several spikes, some of them result from wavefront folding. Some others are due to the microphone resonance, as it is the case for the reference waveform plotted in Fig. 2. However, since the resonance periods of the microphones are known, it was possible to identify separate peak arrivals due to wavefront folding. The two peak pressure lines associated to these

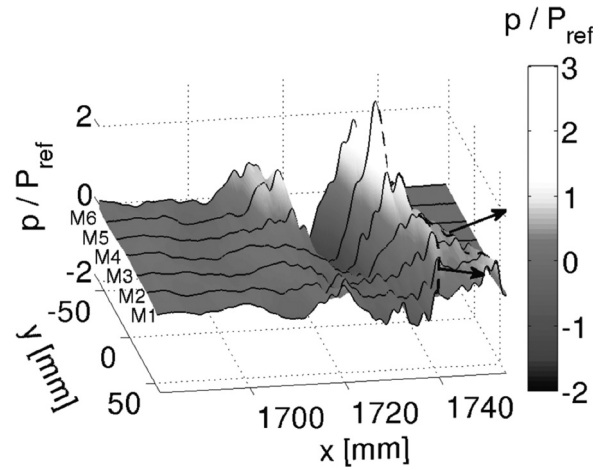


FIG. 6. Pressure field near a focus, measured using a line array of seven microphones M1 to M7 separated by 2 cm in  $y$ -direction (propagation from left to right in  $x$ -direction). The gray scale represents the normalized pressure  $p(x, y)/P_{\text{ref}}$ . —: waveforms measured by the seven microphones. Dashed lines: identified wavefronts and arrows to indicate the propagation direction.

arrivals were plotted with dashed lines in Fig. 6. This figure is consistent with the assumption of wavefront folding in the vicinity of the focus area, as expected from numerical simulations<sup>30</sup> and experiments in water.<sup>6</sup>

## B. Peak pressure statistics

As seen in the previous section, an initial  $N$ -wave can be highly distorted after propagation in the turbulent field, and random attenuation or focusing of the incident  $N$ -wave leads to waves with either amplified or attenuated peak pressures (Fig. 4). In order to analyze the statistics of the positive peak pressure  $P_{\text{max}}$  as a function of propagation distance, waves were recorded for increasing source-microphone distances  $r$  from 250 to 1750 mm. For each distance, 2000 spark shots were recorded using seven microphones, and the statistics were computed.

### 1. Mean effects of turbulence

The mean value and the standard deviation of the measured positive peak pressures normalized by the reference value  $P_{\text{ref}}$  measured without turbulence were plotted in Fig. 7. It is seen that, on average, the effect of the thermal turbulence layer is the attenuation of the peak pressure of the wave. This effect is stronger for longer distances: at a distance  $r = 250$  mm,  $\langle P_{\text{max}} \rangle / P_{\text{ref}} = 0.95$ , and at  $r = 1750$  mm,  $\langle P_{\text{max}} \rangle / P_{\text{ref}} = 0.80$ . Together with the attenuation, an increase of the peak pressure variability with the distance is also observed. Thus, for some waves the peak pressure was amplified by turbulence due to focusing effects, as seen previously in Fig. 6, even at a long distance from the source. This result is consistent with previous studies, which have also shown the higher impact of turbulence with higher turbulence level.<sup>8–11,31</sup>

### 2. Peak pressure distribution

In order to analyze the probability distribution of the pressure level as a function of the propagation distance, the

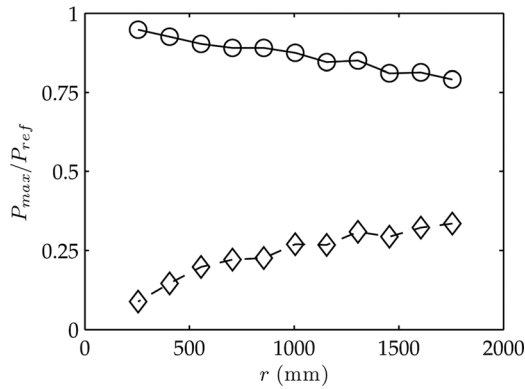


FIG. 7.  $\circ$ : mean value,  $\diamond$ : standard deviation of the peak pressure amplification or attenuation by turbulence as functions of the distance:  $P_{\max}(r)/P_{\text{ref}}(r)$ .

maximum peak pressure distributions were computed for each propagation distance. To analyze the results, it is convenient to define for each propagation distance a variable  $P^*$  as the normalized maximum peak pressure, that is  $P^* = P_{\max}/\langle P_{\max} \rangle$ , the peak pressure value divided by the statistical average at the considered distance. Results were plotted as normalized histograms for four distances (Fig. 8). At the distance  $r = 400$  mm, the distribution is nearly symmetrical, and centered on the mean value. For increasing distances up to  $r = 1750$  mm, waveforms with a peak pressure amplified by a factor of up to 3 were observed, as a result the distribution is less symmetrical and a long tail is formed at high amplitudes. Amplified waves occurred far less frequently than attenuated ones. A similar evolution of the shape of the pressure amplitude distribution for increasing propagation distance through thermal turbulence has been observed previously in the case of linear harmonic waves.<sup>32</sup>

In the case of  $N$ -waves propagating through kinematic turbulence, a similar evolution of the amplitude distributions has also been observed when the intensity of turbulence is increased.<sup>9,10</sup> Following previous works,<sup>32–34</sup> Averiyanov has shown that a generalized gamma distribution whose

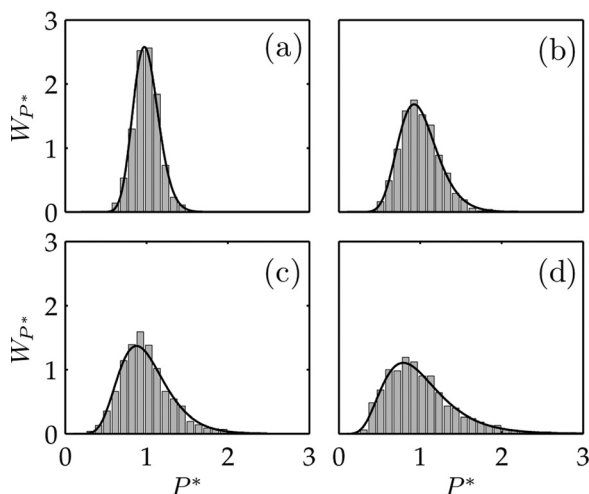


FIG. 8. Probability densities  $W_{P^*}$  of the normalized positive peak pressure  $P^* = P_{\max}/\langle P_{\max} \rangle$  for four distances: (a)  $r = 400$  mm, (b)  $r = 700$  mm, (c)  $r = 1150$  mm, (d)  $r = 1750$  mm. Bar graph: measured values, —: generalized gamma distribution given by Eq. (3).

parameters depend on the turbulence intensity fits the peak pressure distributions with a good agreement.<sup>9</sup> Hereafter it is shown that a similar approach allows the description of the peak pressure distributions with the propagation distance. For the variable  $P^*$ , the generalized gamma distribution is given by Eq. (3)

$$W_{P^*} = \frac{bd^a}{\Gamma(a)} P^{*ab-1} \exp(-dP^{*b}). \quad (3)$$

In this equation,  $\Gamma$  is the gamma function,  $a$  and  $b$  are parameters, and  $d = [\Gamma(a + 1/b)/\Gamma(a)]^b$ . From Eq. (3), the second and third moments  $m_2$  and  $m_3$  are obtained

$$m_2 = \frac{\Gamma(a)\Gamma(a + 2/b)}{\Gamma^2(a + 1/b)}, \quad (4)$$

$$m_3 = \frac{\Gamma^2(a)\Gamma(a + 3/b)}{\Gamma^3(a + 1/b)}. \quad (5)$$

In the case of kinematic turbulence, for a fixed propagation distance, the parameters  $a$  and  $b$  have been found to vary with the root mean square fluctuations of velocity.<sup>9</sup> In the present case of thermal turbulence, for a fixed level of temperature fluctuations, these parameters were found to depend on the propagation distance through the turbulent layer. To estimate the values of  $a$  and  $b$  for a given distance, the system of nonlinear Eqs. (4) and (5) was solved using for  $m_2$  and  $m_3$  the values of the second and third moments of  $P^*$  obtained from the measured dataset at this distance ( $m_2 = \langle P^{*2} \rangle$  and  $m_3 = \langle P^{*3} \rangle$ ). Using this method for each distance, the values of the parameters  $a$  and  $b$  were obtained (Fig. 9). Then, polynomial functions were used to estimate the values of the parameters  $a$  and  $b$  for any distance between  $r = 400$  mm and  $r = 1750$  mm (Fig. 9).

The probability density functions obtained using Eq. (3) and the estimated values of the parameters  $a$  and  $b$  were compared to experimental data (Fig. 8). An excellent agreement is found between the experimental statistical distribution, and the generalized gamma distribution. A practical advantage of this method is that, once the coefficients  $a$  and  $b$  are obtained from measurements at a limited number of source-microphone distances, then the statistical distributions at distances where measurements were not performed can be predicted using Eq. (3) with the appropriate values of  $a$  and  $b$ .

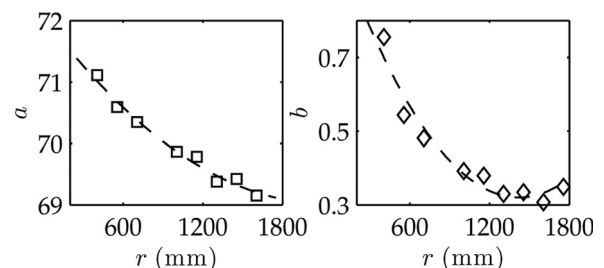


FIG. 9. Coefficients of the generalized gamma distribution as functions of the propagation distance.  $\square$ :  $a$  (left),  $\diamond$ :  $b$  (right), computed from the experimental second and third moments of  $P^*$ , — —: second-order polynomial fit.

Compared to previous studies,<sup>9,35</sup> it is remarkable that increasing the propagation distance or increasing the turbulence intensity leads to a similar evolution of the peak pressure statistics. However, in both cases the dependence of the parameters  $a$  and  $b$  upon the characteristics of the turbulence, the propagation distance, and the wave parameters is not known. Forthcoming studies of the propagation of  $N$ -waves through turbulence based on numerical simulations could give some information on this dependence.

### 3. Peak pressure tail distribution

The tail of the distribution that corresponds to amplified peak pressure was found to be longer for longer propagation distances (Fig. 8). The tail is clearly related to the focusing of  $N$ -waves by the turbulence. The most probable distance  $r_{\text{caus}}$  where the first caustic can be observed has been calculated by Blanc-Benon<sup>32</sup> in the case of linear acoustics using the three-dimensional geometrical acoustics approximation for plane waves propagating through a turbulence described by a Gaussian spectrum:  $r_{\text{caus}} = (L_0/2)(3\beta/\sqrt{\pi}\mu_{\text{rms}}^2)^{1/3}$ , where  $L_0$  is the outer scale of turbulence,  $\mu_{\text{rms}}$  is the root-mean-square fluctuation of refraction index, and  $\beta = 0.33$  is a numerical constant. With the parameters of the present experiment ( $L_0 = 15$  cm and  $\mu_{\text{rms}} = 0.8\%$ ), the most probable distance of occurrence of the first caustic would be  $r_{\text{caus}} = 1540$  mm. However, in the present case, waves are spherical  $N$ -waves propagating through fully developed thermal turbulence described by a von Kármán turbulence model. The application of the previous formula for  $r_{\text{caus}}$  therefore only gives an order of magnitude.

In order to detect the occurrence of focused waves in experimental data, it is interesting to analyze the tail of the peak pressure probability distributions. For this purpose, we defined the tail probability as the probability that the peak pressure normalized by the reference pressure measured without turbulence,  $P_{\text{max}}/P_{\text{ref}}$ , exceeds a given threshold  $\alpha$ , with  $\alpha = 1, 1.5, \text{ or } 2$ . Results obtained using this definition are given in Table II. It was found that the probability  $w(1)$  to observe a wave whose amplitude is greater than the amplitude of the  $N$ -wave in quiescent air is almost constant along the propagation distance, on the order of 20% – 25%. The probability  $w(1.5)$  to observe a 50% increase of the amplitude increases continuously with the propagation distances.

TABLE II. Probability  $w(\alpha)$  for the normalized peak pressure  $P_{\text{max}}/P_{\text{ref}}$  to exceed some threshold  $\alpha$ , with  $\alpha = 1, 1.5, \text{ or } 2$ .

$r$ (mm)	$w(1)$ (%)	$w(1.5)$ (%)	$w(2)$ (%)
250	19.7	0.00	0.00
400	25.7	0.17	0.00
550	26.3	0.45	0.01
700	25.9	0.64	0.02
850	27.6	0.80	0.02
1000	25.5	1.74	0.13
1150	23.9	1.91	0.14
1300	23.1	2.92	0.38
1450	22.4	3.26	0.38
1600	20.5	3.61	0.54
1750	20.0	3.46	0.60

The probability  $w(2)$  to observe peak pressures higher than twice the reference peak pressure without turbulence is significant only starting from  $r > 1000$  mm. A rapid growth of  $w(2)$  from  $r \simeq 1000$  mm is consistent with the formation of caustics by turbulence starting from  $r \simeq 1000$  mm from the source. In the following, an amplification factor  $\alpha = 2$  will be considered as a threshold to register the appearance of caustics near the microphone line. At a long distance, a strong focusing would be unlikely due to the loss of coherence in the acoustic field. One can thus expect that the tail probability  $w(2)$  should saturate and achieve a maximum at some distance. This was not observed in the present experiment. However, a decrease of  $w(2)$  has been observed for propagation distances longer than 2 m during a similar experiment with longer propagation distances.<sup>11</sup>

### C. Width of the focus zones

In this section, the aim is to characterize the width (in  $y$ -direction) of the focus zones after propagation through turbulence. The width of a focus zone, named  $\Delta y_{\text{focus}}$ , is defined here as the width of the area where the pressure field is higher than twice or more the reference peak pressure  $P_{\text{ref}}$ , that is where  $p(x, y)/P_{\text{ref}} > 2$ . From numerical simulations,<sup>14,25,28</sup> an increase of  $\Delta y_{\text{focus}}$  with the distance is expected until caustics are formed. Then,  $\Delta y_{\text{focus}}$  is on the order of the acoustic wavelength, and then it decreases with the distance. The length of the focus zone, named  $\Delta x_{\text{focus}}$ , defined in the similar way, is on the order of 5 to 20 wavelengths.

In the present experiment, for each position 2000 sparks were generated, and waves were simultaneously recorded by the seven microphones. A series of measurements was done with the microphones separated by 10 mm, and another one with the microphones separated by 20 mm. Thus, even if rarely observed, the large number of recordings allowed observing random focusing in some cases. The estimation of  $\Delta x_{\text{focus}}$  would have required the measurement of the wave along the propagation path, which was not possible, but it was possible to estimate  $\Delta y_{\text{focus}}$  for fixed source-microphone distances by using the simultaneous recordings by the seven microphones aligned along the  $y$ -axis. When peak pressures higher than twice the reference peak pressure  $P_{\text{ref}}$  were recorded, it was considered that the microphones were close to a focus zone, and the width  $\Delta y_{\text{focus}}$  was estimated. For this purpose, as previously done for Fig. 6, time waveforms were first converted into pressure field using the sound celerity, and linear interpolation was assumed in  $y$ -direction to estimate the pressure field from the simultaneous recordings by the seven microphones. The width  $\Delta y_{\text{focus}}$  of the area where  $p/P_{\text{ref}} > 2$  was then obtained (see, for example, Fig. 10, which is a top view of Fig. 6). This processing was repeated for all source-microphone distances. The average value  $\langle \Delta y_{\text{focus}} \rangle$  was computed for each source-microphone distance by considering only the recordings such as at least one microphone registered a maximum peak pressure higher than  $2P_{\text{ref}}$ . The average width  $\langle \Delta y_{\text{focus}} \rangle$  was plotted as a function of distance in Fig. 11. For short propagation distances  $r < 400$  mm,  $w(2) = 0$  (see Table II) thus it is considered that no focus was observed. For intermediate propagation distances between  $r = 550$  mm

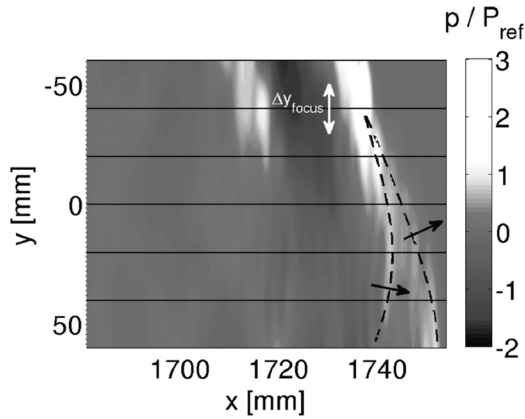


FIG. 10. Pressure field near a focus (top view of Fig. 6). The width  $\Delta y_{\text{focus}}$  of the focus zone is defined as the width where  $p/P_{\text{ref}} > 2$ . Dashed lines and associated arrows show the wavefronts as shown in Fig. 6.

and  $r = 1000$  mm,  $\langle \Delta y_{\text{focus}} \rangle$  increases with the distance. For these distances, the probability to observe the doubling of the pressure level is small [ $0 < w(2) < 0.4$ ], actually  $\langle \Delta y_{\text{focus}} \rangle$  was estimated from only 2 or 3 pressure fields. For propagation distances longer than 1000 mm,  $\langle \Delta y_{\text{focus}} \rangle$  is nearly constant, and the value is on the order of the initial wavelength (20 mm). It is clear that the estimation of  $\langle \Delta y_{\text{focus}} \rangle$  was not accurate because the distance between the microphones is large (10 or 20 mm). However, the fact that the width of focus zones was found to be on the order of the wavelength is consistent with numerical simulations of  $N$ -wave propagation through turbulence.<sup>25,28</sup>

#### D. Angle of deviation

As shown in Fig. 6 and Fig. 10 with arrows, by analyzing the time difference of arrival on the seven microphones it was possible to estimate the propagation direction of incident waves and, therefore, the angle of arrival. In numerical simulations of wave propagation based on the solution of a parabolic equation, it is usually assumed that the deviation from the main propagation axis induced by turbulence is smaller than  $15^\circ$ . In order to check that the angle of deviation remains enough small to allow the application of such method to model this kind of laboratory-scale experiment, the angle of deviation after propagation through turbulence was analyzed.

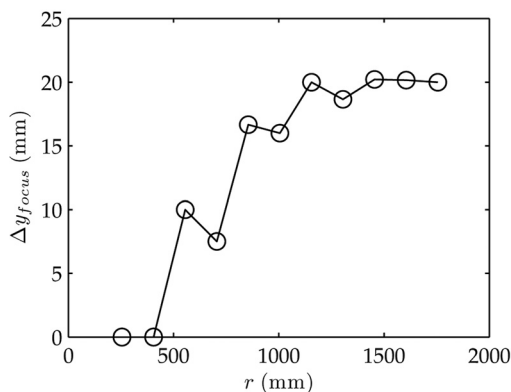


FIG. 11. Statistical average  $\langle \Delta y_{\text{focus}} \rangle$  of the width of the focus regions  $\Delta y_{\text{focus}}$ , as a function of distance  $r$ .

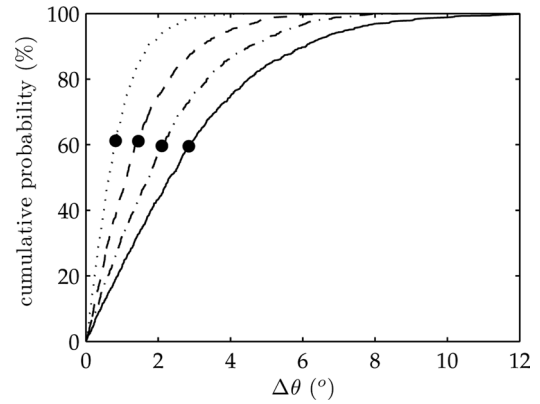


FIG. 12. Cumulative probability distribution of the deviation angle  $\Delta\theta$  for four distances:  $\cdots$ ,  $r = 400$ ,  $---$ ,  $r = 700$ ,  $- \cdot - \cdot -$ ,  $r = 1150$ , and  $---$ ,  $r = 1750$  mm).  $\bullet$ : mean value  $\langle \Delta\theta \rangle$ .

The reference axis for the measurement of the angle of deviation is the line from the source to the microphone at the center of the baffle (microphone no. 4). The baffle being mounted on a rotation stage, its positioning was accurately controlled. The distance between neighbor microphones was 1 cm. Without turbulence, the angle of arrival obtained from the time difference of arrival was found to be less than 1 deg. With turbulence, the angle of arrival was estimated for eleven source-microphone distances (from  $r = 250$  to 1750 mm) and 1000 recordings per distance. Then, the statistics of  $\Delta\theta$ , defined as the absolute value of the angle of deviation induced by turbulence, were computed. Cumulative probability distributions of  $\Delta\theta$  are given in Fig. 12 for four distances ( $r = 400, 700, 1150, 1750$  mm). For  $r = 250$  to 1750 mm, it has been found that the mean value of the angle of deviation  $\langle \Delta\theta \rangle$  increases from  $0.5^\circ$  to  $2.8^\circ$ , the standard deviation increases from  $0.5^\circ$  to  $2.3^\circ$ . The maximum value also increases with the distance: from  $3^\circ$  to  $12.4^\circ$ . However, between 99% and 100% of the deviation angle values were smaller than  $10^\circ$ , whatever the distance (Fig. 12). This preliminary analysis confirms that the angle of deviation remained sufficiently small to consider that the paraxial approximation is valid, which allows the use of parabolic equation method to model this kind of experiment.<sup>25,36</sup>

#### E. Rise time

The rise time of the front shock is the second important parameter that affects the perceived level of sonic booms.<sup>37</sup> The atmospheric turbulence is known to be responsible for the increase of the front shock rise time of sonic booms observed in the atmosphere.<sup>38,39</sup> At the laboratory scale, it has also been observed that turbulence increases the rise time of spark-generated  $N$ -waves.<sup>9-11,40</sup> But one can also expect that nonlinear effects induce a decrease of the rise time at caustics because the pressure level can be amplified by a factor of three or more at focus.

Concerning laboratory-scale experiments, the rise time analysis must be done carefully because the limited frequency response of commercially available condenser microphones does not allow the measurement of rise times shorter than  $2.6 \mu\text{s}$ . In the case of strongly distorted waves [see Fig. 4(b) for example], the rise time estimation is not obvious, and different

methods of estimation can be used. The following discussion is limited to the front shock *standard* rise time, defined as the duration of the pressure rise from 10% to 90% of the positive peak. Since 1/8-in. condenser microphones were used, the  $-3$  dB cut-off was around 140 kHz, and consequently the minimum value of the rise time deduced from the microphone output voltage is longer than  $2.6 \mu\text{s}$ . This limitation has already been mentioned both in studies on blast waves<sup>22</sup> or spark-generated *N*-waves.<sup>18</sup> To overcome this limitation, Yuldashev<sup>13</sup> has developed an optical method based on the analysis of shadowgraphs that allowed the measurement of rise times as small as  $0.3 \mu\text{s}$ . This value is ten times smaller than the value obtained from the microphone output voltage. The practical consequence of this result is that it is not meaningful to discuss the statistics of the smallest rise times obtained from 1/8-in. microphones, and only the increase of the rise time can be discussed. Thus, contrary to what was done for the maximum peak pressure (see Sec. III B), it was not possible to use the present experimental data to propose a statistical law that would fit the distribution of rise times obtained with turbulence.

In Fig. 13, the average value  $\langle \tau \rangle$  and the standard deviation  $\sigma_\tau$  of the rise time  $\tau$  were plotted as functions of distance  $r$ . At a distance  $r = 250$  mm, the mean rise time and its standard deviation are equal to the reference values measured without turbulence, the minimum value being on the order of  $2.6 \mu\text{s}$ . With increasing distance  $r$ , the mean rise time increases, as was observed in similar studies.<sup>9-11</sup> At the distance  $r = 1750$  mm, the mean rise time was found to be about  $7.3 \mu\text{s}$  with a standard deviation of  $5 \mu\text{s}$ . At this distance, larger than the caustic formation distance, some long rise times do actually correspond to smoothed wavefronts. However, in many cases, multiple peaks occur during the pressure rise due to wavefront folding. Then, like for the waveform in Fig. 4(b), measuring the rise time between 10% and 90% of the peak pressure leads to large values of the rise time, even for sharp shock fronts.

The probability densities  $W_\tau$  of the rise time  $\tau$  were plotted in Fig. 14 for distances  $r = 400, 700, 1150,$  and  $1750$  mm. As expected, we observe a broadening of the density probability  $W_\tau$ , together with a decrease in the probability amplitude and the appearance of a tail at large rise times. For example, rise times of up to  $20 \mu\text{s}$  were observed at long distances, whereas it

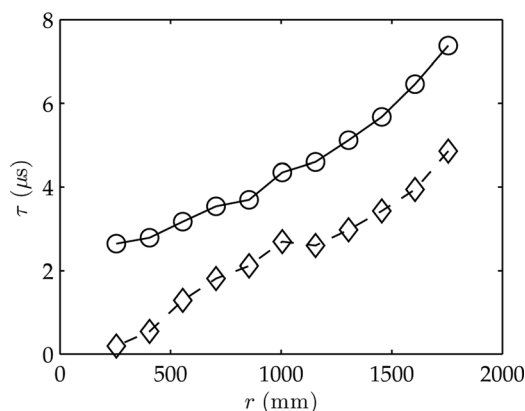


FIG. 13.  $\circ$ : mean value,  $\diamond$ : standard deviation of the front shock rise time  $\tau$ , as functions of distance  $r$ .

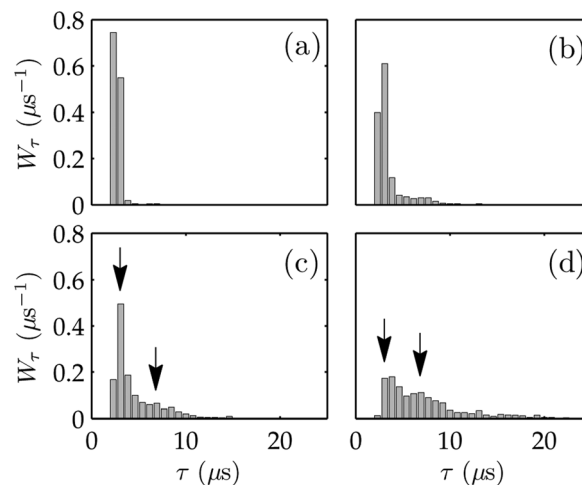


FIG. 14. Probability densities  $W_\tau$  of the front shock rise time for four distances: (a)  $r = 400$  mm, (b)  $r = 700$  mm, (c)  $r = 1150$  mm, (d)  $r = 1750$  mm. Arrows indicate two groups of data, which depend on the microphone response as detailed in the Appendix.

has been found to be less than  $1 \mu\text{s}$  in a quiescent air.<sup>13</sup> In the context of the sonic boom, a significant increase of the shock rise time is a positive effect since waves with smoothed front shocks are perceived less loudly.<sup>41</sup> Two local maxima are seen on the statistical distributions, close to the values  $\tau = 3 \mu\text{s}$  and  $\tau = 7 \mu\text{s}$  as indicated with arrows in Fig. 14. Actually, the same two maxima appeared on all rise time distributions, whatever the propagation distance  $r$  was. These maxima are artifacts caused by the microphone response. It was indeed found that there is a higher probability to measure rise times on the order of the microphone rise time ( $\approx 3 \mu\text{s}$ ) or values close to  $7 \mu\text{s}$ , which correspond to the period of the oscillations seen on the microphone output voltage (see Fig. 2). In order to show that using a different type of microphone would lead to partly different statistical distributions, an additional series of recordings was done using a 1/4-in. microphone (Brüel & Kjær type 4939) and an 1/8-in. microphone (Brüel & Kjær type 4138) at the same time. Results are reported in the Appendix.

#### IV. CONCLUSION

The propagation of high-amplitude acoustic *N*-waves through a thermal turbulence was experimentally studied at the laboratory scale. The influence of the propagation distance through thermal turbulence on the positive peak pressure and on the rise time of the pressure waves was investigated. A full range of distorted waveforms was measured. In particular, *U*-waves associated to *N*-wave focusing were observed. Spiked waves with multiple arrivals were observed in the vicinity of the focus regions. The width of the focus zones was estimated for increasing distances. This width is on the order of the acoustic wavelength as predicted by numerical simulations.<sup>25</sup>

The effects of turbulence on the statistics of the positive peak pressure were observed for increasing distances. Similarly to previous studies in kinematic or thermal turbulence,<sup>8,9,11</sup> on average, the effect of turbulence is an attenuation of the peak pressure level. Attenuation by turbulence is more effective with the propagation distance. Probability

distributions were computed from thousands of waves. It was shown that the probability density function of peak pressure can be approximated using a generalized gamma distribution with an excellent agreement. The parameters of this probability law were found to be functions of the propagation distance. A practical consequence of this result is that the knowledge of the statistical distribution for a finite number of propagation distances permits to deduce the statistics at intermediate distances. This result complements the result of Averiyarov,<sup>9</sup> who similarly found that the peak pressure statistical distributions, after propagation through kinematic turbulence for a fixed distance, can be described by generalized gamma distributions whose parameters vary with the turbulence level. However, in both cases, the dependence of the statistical distribution parameters on the wave and on the turbulence characteristics is not yet theoretically established, and their values still have to be deduced from experimental data. Numerical simulations of the propagation through thermal turbulence would help to understand this dependence.

Concerning the variability of the propagation direction of waves, a preliminary study confirms that the deviation from the main propagation direction remains small enough to allow the use of the paraxial approximation to model this kind of laboratory-scale experiment.

The limited bandwidth of the microphones did not allow the measurement of the smallest front shock rise time values. However, the increase of the rise time by turbulence was clearly observed. This increase of the front shock rise time can be seen as a positive effect of turbulence if considering the sonic boom impact of distorted waveforms. However, one should note that the waves with increased maximum peak pressure level often have a small front shock rise time. These two characteristics contribute to significantly increase the perceived noise level of shock waves. In this study, the influence of the microphone type on the rise time statistics is highlighted: Local maxima, which depend on the microphones' responses, were observed on the probability distributions. In the future, the development of new measurement techniques should enable a more detailed study of the rise time, without the effects related to microphone filtering.

## ACKNOWLEDGMENTS

This work is supported by the French/Russian Program for International Scientific Cooperation PICS RFBR 10-02-91062 / CNRS 5603, and by the Grant of the President of Russia MK-5895.2013.2. This work was performed within the framework of the Labex CeLyA of Université de Lyon, operated by the French National Research Agency (ANR-10-LABX-0060/ ANR-11-IDEX-0007). The authors thank Jean-Michel Perrin and Emmanuel Jondeau for their help during the experiment.

## APPENDIX: INFLUENCE OF THE MICROPHONE RESPONSE ON THE RISE TIME STATISTICS

In order to highlight the influence of the microphone response on the rise time statistics, 2000 waves were simultaneously recorded using two different types of microphone,

both from Brüel & Kjær company. One is an 1/8-in. type 4138 as used previously, and the second is a 1/4-in. type 4939. Both were connected to the same Brüel & Kjær Nexus modified amplifier ( $-3$  dB cutoff at 200 kHz). Since both microphones are mounted at normal incidence, differences in measured data are due to their different responses (i.e., different rise time, high frequency cutoff, and resonance frequency). Pressure waves have been recorded at a distance  $r = 1750$  mm from the spark source, first without turbulence, then after propagation through the turbulent layer. As previously defined, the reference value  $P_{\text{ref}}$  is the mean value of the peak pressure level obtained without turbulence. Results were plotted in Fig. 15 as scatter plots of the normalized peak pressure  $P_{\text{max}}/P_{\text{ref}}$  as a function of rise time, for every single wave. In these figures, crosses represent measurements with turbulence, whereas measurements without turbulence are indicated as dots. Two groups of data are identified using arrows. For the 1/8-in. microphone [Fig. 15(a)], a first group of data is centered close to  $\tau = 2.7 \mu\text{s}$ , which is the rise time of this microphone. Similarly for the 1/4-in. microphone [Fig. 15(b)], a group of data is centered close to  $\tau = 4 \mu\text{s}$ , which is the rise time of this microphone. For each microphone, a second group of data is found at a time close to the period of oscillations seen on the microphone output voltage (Fig. 2), at  $\tau = 7 \mu\text{s}$  approximately for the 1/8-in. microphone, and  $\tau = 12 \mu\text{s}$  for the 1/4-in. microphone. In order to check that these differences are induced by the microphones' responses, the waveforms obtained with the 1/8-in. microphone were filtered using a filter that models the frequency response of the 1/4-in. microphone provided by the manufacturer, then the rise times of the

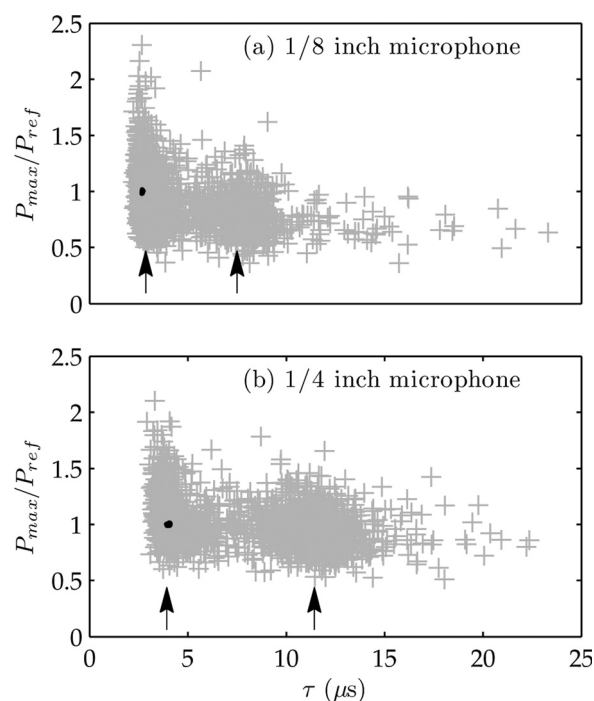


FIG. 15. Normalized peak pressure  $P_{\text{max}}/P_{\text{ref}}$  as a function of rise time  $\tau$  at a distance  $r = 1750$  mm: (a) measured with an 1/8-in. condenser microphone and (b) measured with a 1/4-in. condenser microphone. +: with turbulence,  $\bullet$ : without turbulence. Arrows indicate two groups of data, which depend on the microphone response.

filtered waves were computed. The resulting distribution of data (not shown in this paper) has two groups of data centered on the same values as the ones obtained using the 1/4-in. microphone output.<sup>15</sup> This analysis confirms that the response of the microphones have a great influence on the measured statistical distribution of rise time values, and not only on the smallest values. This effect therefore has to be taken into account when analyzing data from laboratory-scale experiments based on spark-generated waves. As spark-generated pressure waves have energy content at frequencies up to 1 MHz, a similar behavior is expected with any commercially available condenser microphone.

- <sup>1</sup>D. Maglieri, "Sonic boom flight research - some effects of airplane operations and the atmosphere on sonic boom signatures," NASA [Spec. Publ.] SP **147**, 25–48 (1967).
- <sup>2</sup>R. Raspet, H. Bass, L. Yao, P. Boulanger, and W. McBride, "Statistical and numerical study of the relationship between turbulence and sonic boom characteristics," J. Acoust. Soc. Am. **96**, 3621–3626 (1994).
- <sup>3</sup>K. J. Plotkin, D. J. Maglieri, and B. Sullivan, "Measured effects of turbulence on the loudness and waveforms of conventional and shaped minimized sonic booms," in *11th AIAA/CEAS Aeroacoustics Conference* (2005), AIAA 2005–2949.
- <sup>4</sup>J. L. Wanner, J. Vallee, C. Vivier, and C. Thery, "Theoretical and experimental studies of the focus of sonic booms," J. Acoust. Soc. Am. **52**, 13–32 (1972).
- <sup>5</sup>L. L. Locey and V. W. Sparrow, "Modeling atmospheric turbulence as a filter for sonic boom propagation," Noise Control Eng. J. **55**, 495–503 (2007).
- <sup>6</sup>L. Ganjehi, R. Marchiano, and F. Coulouvrat, "Evidence of wave front folding of sonic booms by a laboratory-scale deterministic experiment of shock waves in a heterogeneous medium," J. Acoust. Soc. Am. **124**, 57–71 (2008).
- <sup>7</sup>B. A. Davy and D. T. Blackstock, "Measurements of the refraction and diffraction of a short N-wave by a gas-filled soap bubble," J. Acoust. Soc. Am. **49**, 732–737 (1971).
- <sup>8</sup>B. Lipkens and D. T. Blackstock, "Model experiment to study sonic boom propagation through turbulence. Part I. General results," J. Acoust. Soc. Am. **103**, 148–158 (1998).
- <sup>9</sup>M. Averiyarov, S. Ollivier, V. Khokhlova, and P. Blanc-Benon, "Random focusing of nonlinear acoustic N-waves in fully developed turbulence: Laboratory scale experiment," J. Acoust. Soc. Am. **130**, 3595–3607 (2011).
- <sup>10</sup>B. Lipkens and D. T. Blackstock, "Model experiment to study sonic boom propagation through turbulence. Part II. Effect of turbulence intensity and propagation distance through turbulence," J. Acoust. Soc. Am. **104**, 1301–1309 (1998).
- <sup>11</sup>S. Ollivier and P. Blanc-Benon, "Model experiment to study acoustic N-wave propagation through turbulence," in *10th AIAA/CEAS Aeroacoustics Conference*, Manchester, UK (2004), AIAA 2004–2921.
- <sup>12</sup>P. V. Yuldashev, M. V. Averiyarov, V. A. Khokhlova, S. Ollivier, and P. Blanc-Benon, "Nonlinear spherically divergent shock waves propagating in a relaxing medium," Acoust. Phys. **54**, 32–41 (2008).
- <sup>13</sup>P. V. Yuldashev, S. Ollivier, M. V. Averiyarov, O. Sapozhnikov, V. A. Khokhlova, and P. Blanc-Benon, "Nonlinear propagation of spark-generated N-waves in air: Modeling and measurements using acoustical and optical methods," J. Acoust. Soc. Am. **128**, 3321–3333 (2010).
- <sup>14</sup>P. V. Yuldashev, "Nonlinear shock waves propagation in random media with inhomogeneities distributed in space or concentrated in a thin layer," Ph.D. thesis, École Centrale de Lyon, N° 2011-34, 2011.
- <sup>15</sup>E. Salze, "Propagation acoustique non-linéaire en atmosphère inhomogène avec effets de sol: expériences à l'échelle du laboratoire (Nonlinear sound propagation in an inhomogeneous atmosphere: laboratory-scale experiments)," Ph.D. thesis, École Centrale de Lyon, N° 2012-38, 2012 (in French).
- <sup>16</sup>W. Wright and N. Medendorp, "Acoustic radiation from a finite line source with N-wave excitation," J. Acoust. Soc. Am. **43**, 966–971 (1968).
- <sup>17</sup>R. Klinkowstein, "A study of acoustic radiation from an electrical spark discharge in air," Master's thesis, Massachusetts Institute of Technology, 1974.
- <sup>18</sup>W. Wright, "Propagation in air of N-waves produced by sparks," J. Acoust. Soc. Am. **73**, 1948–1955 (1983).
- <sup>19</sup>H. Honma, I. Glass, C. Wong, O. Holst-Jensen, and D. Xu, "Experimental and numerical studies of weak blast waves in air," Shock Waves **1**, 111–119 (1991).
- <sup>20</sup>M. Wochner, A. Atchley, and V. Sparrow, "Numerical simulation of finite amplitude wave propagation in air using a realistic atmospheric absorption model," J. Acoust. Soc. Am. **118**, 2891–2898 (2005).
- <sup>21</sup>E. Salze, S. Ollivier, P. Blanc-Benon, P. Yuldashev, M. Averiyarov, and V. Khokhlova, "Characterization of the sound field emitted by an electric spark source in air," in *Forum Acusticum*, Aalborg, Denmark (2011), Acusticum/285, CD-rom ISSN 2221-3767.
- <sup>22</sup>A. Loubeau, V. Sparrow, L. Pater, and W. Wright, "High-frequency measurements of blast wave propagation," J. Acoust. Soc. Am. **120**, 29–34 (2006).
- <sup>23</sup>C. Bailly and G. Comte-Bellot, *Turbulence* (CNRS Éditions, 2003) (in French).
- <sup>24</sup>D. Wilson, J. Brasseur, and K. Gilbert, "Acoustic scattering and the spectrum of atmospheric turbulence," J. Acoust. Soc. Am. **105**, 30–34 (1999).
- <sup>25</sup>M. Averiyarov, P. Blanc-Benon, R. Cleveland, and V. Khokhlova, "Nonlinear and diffraction effects in propagation of N-waves in randomly inhomogeneous moving media," J. Acoust. Soc. Am. **129**, 1760–1772 (2011).
- <sup>26</sup>G. Herbert, W. Hass, and J. Angell, "A preliminary study of atmospheric effects on the sonic boom," J. Appl. Meteorol. **8**, 618–626 (1969).
- <sup>27</sup>F. Coulouvrat, "Focusing of weak acoustic shock waves at a caustic cusp," Wave Motion **32**, 233–245 (2000).
- <sup>28</sup>R. Marchiano and F. Coulouvrat, "Numerical simulation of shock wave focusing at fold caustics, with application to sonic boom," J. Acoust. Soc. Am. **114**, 1758–1771 (2003).
- <sup>29</sup>L. Hesselink and B. Sturtevant, "Propagation of weak shocks through a random medium," J. Fluid Mech. **196**, 513–553 (1988).
- <sup>30</sup>A. Piacsek, "Atmospheric turbulence conditions leading to focused and folded sonic boom wave fronts," J. Acoust. Soc. Am. **111**, 520–529 (2002).
- <sup>31</sup>S. Ollivier and P. Blanc-Benon, "Numerical simulation of 'low level' sonic boom propagation through random inhomogeneous sound speed fields," in *19th International Congress on Acoustics*, Madrid (2007).
- <sup>32</sup>P. Blanc-Benon, D. Juvé, V. Ostashev, and R. Wandelt, "On the appearance of caustics for plane sound-wave propagation in moving random media," Waves Random Media **5**, 183–199 (1995).
- <sup>33</sup>T. Ewart and D. Perceival, "Forward scattered waves in random media—The probability distribution of intensity," J. Acoust. Soc. Am. **80**, 1745–1753 (1986).
- <sup>34</sup>T. Ewart, "A model of the intensity probability distribution of for wave propagation in random media," J. Acoust. Soc. Am. **86**, 1490–1498 (1989).
- <sup>35</sup>P. Blanc-Benon and D. Juvé, "Intensity fluctuations of spherical acoustic waves propagating through thermal turbulence," Waves Random Media **3**, 71–83 (1993).
- <sup>36</sup>P. Blanc-Benon, B. Lipkens, L. Dallois, M. Hamilton, and D. Blackstock, "Propagation of finite amplitude sound through turbulence: Modeling with geometrical acoustics and the parabolic approximation," J. Acoust. Soc. Am. **111**, 487–498 (2002).
- <sup>37</sup>A. Niedzwiecki and H. Ribner, "Subjective loudness of N-wave sonic boom," J. Acoust. Soc. Am. **64**, 1617–1621 (1978).
- <sup>38</sup>A. George and K. Plotkin, "Propagation of sonic booms and other weak nonlinear waves through turbulence," Phys. Fluids **14**, 548–554 (1971).
- <sup>39</sup>A. Pierce, "Statistical theory of atmospheric turbulence effects on sonic-boom rise times," J. Acoust. Soc. Am. **49**, 906–929 (1971).
- <sup>40</sup>P. Blanc-Benon and S. Ollivier, "Model experiments to study acoustic N-waves propagation through turbulence," in *1st International Symposium on Long Range Sound Propagation*, Fairlee, VT (2004). <http://nca.olemiss.edu/long-range-sound-propagation-lrsp/> (Last viewed 04/10/2013).
- <sup>41</sup>S. Fidell, L. Silvati, and K. Pearsons, "Relative rates of growth of annoyance of impulsive and non-impulsive noises," J. Acoust. Soc. Am. **111**, 576–585 (2002).